Enhancing the heralded single-photon rate from a silicon nanowire by time and wavelength division multiplexing pump pulses

X. Zhang,[1] I. Jizan,[1] J. He,[1] A. S. Clark,[1,2] D.-Y. Choi,[3] C. J. Chae,[4] B. J. Eggleton,[1] and C. Xiong[1,*]

[1]Centre for Ultrahigh bandwidth Devices for Optical Systems (CUDOS), Institute of Photonics and Optical Science (IPOS), School of Physics, University of Sydney, NSW 2006, Australia

[2]Centre for Cold Matter, Blackett Laboratory, Imperial College London, London SW7 2AZ, UK

[3]CUDOS, Laser Physics Centre, Australian National University, Canberra, ACT 2601, Australia

[4]Advanced Photonics Research Institute, Gwangju Institute of Science and Technology, Gwangju, South Korea

*Corresponding author: chunle@physics.usyd.edu.au

Received February 23, 2015; revised April 28, 2015; accepted April 30, 2015; posted May 1, 2015 (Doc. ID 234924); published May 19, 2015

Heralded single photons produced on a silicon chip represent an integrated photon source solution for scalable photonic quantum technologies. The key limitation of such sources is their non-deterministic nature introduced by the stochastic spontaneous four-wave mixing (SFWM) process. Active spatial and temporal multiplexing can improve this by enhancing the single-photon rate without degrading the quantum signal-to-noise ratio. Here, taking advantage of the broad bandwidth of SFWM in a silicon nanowire, we experimentally demonstrate heralded single-photon generation from a silicon nanowire pumped by time and wavelength division multiplexed pulses. We show a $90 \pm 5\%$ enhancement on the heralded photon rate at the cost of only $14 \pm 2\%$ reduction to the signal-to-noise ratio, close to the performance found using only time division multiplexed pulses. As single-photon events are distributed to multiple wavelength channels, this new scheme overcomes the saturation limit of avalanche single-photon detectors and will improve the ultimate performance of such photon sources. © 2015 Optical Society of America

OCIS codes: (270.0270) Quantum optics; (190.0190) Nonlinear optics; (190.4380) Nonlinear optics, four-wave mixing; (130.0130) Integrated optics.

http://dx.doi.org/10.1364/OL.40.002489

Integrated single-photon sources are one of the core components for photonic quantum computation [1] and quantum communication [2]. One popular approach to produce single photons from an integrated platform is to use nonlinear processes, such as spontaneous parametric downconversion (SPDC) [3,4] or spontaneous four-wave mixing (SFWM) [5–11], in nonlinear optical waveguides to generate correlated photon pairs. The detection of one photon (heralding photon) from a pair indicates the existence of its partner photon (heralded photon), forming a heralded single-photon source.

Some applications require a high rate of heralded single photons from one source, and many others need the interference between single photons from two or more separate sources. Given an average number of pairs generated per pump pulse μ, a pump-pulse repetition rate R, and a photon collection and detection efficiency η, the heralded photon rate of one source is $\mu\eta^2 R$, and the number of interference events per second is $\mu^2\eta^4 R$ in the case that involves only two sources. To have fast operation in all of these applications, we need to increase μ, η, and $R \cdot \eta$ is related to losses and detector efficiencies and is thus eventually determined by fabrication technologies. Improving μ is very challenging because of the statistical nature of photon emission via a spontaneous nonlinear process, in which it is almost impossible to simultaneously produce single pairs at a high probability while suppressing the probability of emitting multi-pair noise. The situation has changed since the schemes of active spatial and temporal multiplexing were introduced [12,13]. In these schemes, μ can be enhanced while the quantum signal to noise ratio remains the same. The ultimate performance of these multiplexing schemes is determined by the loss and speed of switches, as well as the speed of detectors and electronics that control the switches [13–16]. An alternative approach is to increase the pump pulse-repetition rate R through time-division multiplexing (TDM), in which no switch is required [17]. However with the increase of R, an avalanche photon detector (APD) working in the telecom band can be saturated quickly because of the long deadtime and thus limit the ultimate performance and scalability. One possible solution is to replace APDs with complex superconducting single-photon detectors (SSPDs) that have much shorter deadtime and higher saturation margin. In this Letter, we propose and experimentally demonstrate a very effective scheme that is based on time and wavelength division-multiplexing (TWDM) of the pump without the need of replacing APDs by complex SSPDs. It has the potential to help achieve higher scalability while avoiding the APD's saturation problem to a large extent.

Figure 1 shows the schematics of only using TDM [Fig. 1(a)] and our proposed TWDM [Fig. 1(b)]. In the TDM scheme shown in Fig. 1(a), the original pulsed pump is at a single wavelength and has a period of NT. Using two 1-to-N couplers and optical delay lines with a delay of $0, T, 2T, \ldots (N-1)T$, the period of the pump becomes T, and the repetition rate R is increased by N times. If the average number of pairs generated per pump pulse μ is the same, the heralded single-photon rate will increase by N times. Because only one APD is used for the heralding arm, the APD will be saturated if R is too high. In our proposed TWDM scheme shown in Fig. 1(b), the original pulsed pump contains

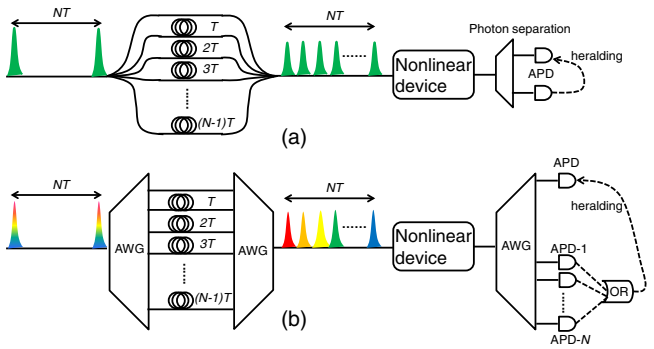

Fig. 1. Schematic diagrams of (a) TDM-, and (b) TWDM-based pump schemes. APD: avalanche photon detector, AWG: arrayed waveguide grating.

N wavelength channels and has a period of NT. Using two arrayed waveguide gratings (AWG) and optical delay lines, the pump rate R is increased by N times as in the TDM case. Because the pump has N wavelength channels, the heralding photons will be distributed to N APDs, and thus the saturation can be avoided. To implement this new scheme, the nonlinear device has to allow broadband SFWM so that all pump channels have similar probability to generate photon pairs and all photon pairs share the same heralded channel. The well-defined AWG channel spacing and channel bandwidth will guarantee that all idler photons generated from different pumps are frequency indistinguishable [18].

In this Letter, we experimentally demonstrate the TWDM scheme shown in Fig. 1(b) with $N = 2$ to enhance the heralded single-photon rate for sources with a broad SFWM bandwidth, in this case a silicon nanowire source. By doubling R, we have achieved $90 \pm 5\%$ enhancement on the heralded single-photon rate at the cost of only $14 \pm 2\%$ reduction to the quantum signal-to-noise ratio.

Keeping the broadband SFWM requirement in mind, we fabricated a 3-mm-long, 220-nm-high and 460-nm-wide silicon nanowire on a silicon-on-insulator wafer with a 2-μm upper-cladding of SiO_2. With the designed dimension, the TE polarization mode of the nanowire exhibited anomalous dispersion in the telecom band [Fig. 2(a)], which was necessary for broadband SFWM. Using the dispersion data and the model in Ref. [19], we calculated the SFWM photon flux as a function of frequency detuning from pump at a typical pump level of $\gamma PL = 0.05$, where γ is the nonlinear coefficient, P is the peak power, and L is the nanowire length. The normalized SFWM photon flux is plotted in Fig. 2(b), which shows that the SFWM bandwidth (half width at half maximum) in this nanowire is over 6 THz.

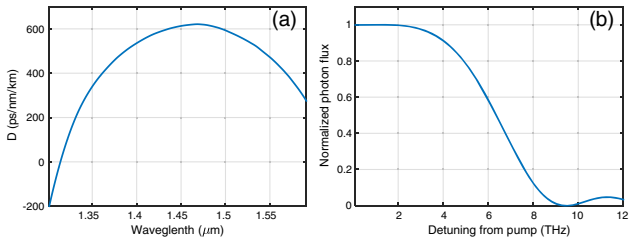

Fig. 2. (a) Calculated dispersion profile for the TE mode of the nanowire. (b) Normalized SFWM photon flux as a function of frequency detuning from pump frequency.

To demonstrate the feasibility of the proposed TWDM scheme, we set up an experiment for $N = 2$ as illustrated in Fig. 3. We pumped the silicon nanowire with two time-division multiplexed pulses, spectrally separated by 0.1 THz [Fig. 3(a)], Pump 1 (P1, lower frequency), and Pump 2 (P2, higher frequency), which were able to generate spectrally overlapped photons. In our experiment, the generated photon pairs from P1 were post-selected at 0.6-THz detuning from P1, and those photon pairs generated from P2 were post-selected at 0.7-THz detuning from P2. The idler photons generated from the two pumps were therefore at the same frequency. Each individual pump had a pulse period of 20 ns, and one was delayed by 10 ns to the other to form a time-division multiplexed pulse train as shown in Fig. 3(b), so that the idler photons from each pump were heralded by their corresponding signal photons. Compared with the experiment using only one pump with 20 ns period, this scheme is equivalent to doubling the pump repetition rate and will therefore enhance the heralded single-photon rate without reducing the coincidence to accidental ratio (CAR)—a measurement of the quantum signal-to-noise ratio [17].

The experimental setup is shown in Fig. 3(c). Two external-cavity diode lasers (ECDL) were used to emit two pumps separated by 0.1 THz (1550.12 nm and 1550.92 nm, respectively). After going through polarization controllers (PC), they were combined by a 50/50 fiber coupler and modulated by a single lithium niobate intensity modulator (IM). The IM was driven by a pulse generator that produced 250-ps-wide Gaussian pulses at 50-MHz repetition rate. The two pumps were then amplified by an erbium-doped fiber amplifier (EDFA). They were separated using a low-loss arrayed waveguide grating (AWG, from JDS Uniphase, 0.1-THz channel spacing and 0.05-THz channel bandwidth). P1 was subsequently

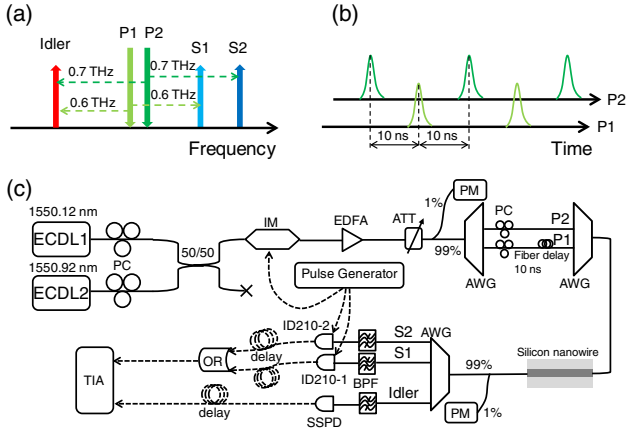

Fig. 3. (a) Wavelength division multiplexing of two pumps separated by 0.1 THz. (b) Time division multiplexing of two pumps: the original period of both pumps was 20 ns, and P1 was delayed by 10 ns from P2. (c) Experimental setup. ECDL: external cavity diode laser, PC: polarization controller, IM: intensity modulator, EDFA: erbium-doped fiber amplifier, ATT: attenuator, PM: power meter, AWG: arrayed waveguide grating, BPF: band pass filter, SSPD: superconducting single-photon detector, and TIA: time-interval analyzer. Solid and dashed lines represent fiber and electronic connections, respectively.

delayed by 10 ns, corresponding to half of the modulation period. After being recombined using another AWG, two pumps were injected into the silicon nanowire. The total insertion loss of the nanowire was as low as 5 dB for the TE mode because of the use of inversed tapers and lensed fibers. PCs were placed in the two pump channels between the two AWGs to adjust the pump polarization independently so that both pumps were TE polarized in the nanowire. The two AWGs also played the role of filters to get rid of amplified spontaneous emission noise from the EDFA as well as any possible spontaneous Raman scattering noise from the connection fibers before them. A tunable attenuator (ATT), 1:99 fiber couplers, and power meters (PM) were used along the optical circuit to control and monitor the pump power. At the output of the nanowire S1 (generated by P1), S2 (generated by P2), and idler photons were separated using the third AWG and further filtered by band-pass filters (BPF). The total loss of the AWG and the BPF was approximately 4.5 dB. The two channels carrying S1 and S2 photons were sent to InGaAs avalanche single-photon detectors (ID210, ID-Quantique, 25% efficiency, 1-ns effective gate width, 20-μs deadtime, gated at 50 MHz by the pulse generator, 1000-Hz dark count), and the idler photons were sent to a SSPD (Single Quantum, 10% efficiency with 100-Hz dark count). In this configuration, the detection of the signal photons generated from both pumps could herald the arrival of an idler photon. The detection signals from the two ID210 detectors were sent to an OR gate. The output of the OR gate and the detection signal of the SSPD were both sent to a time-interval analyzer (TIA) for measurements. The internal tunable trigger delay of the ID210 was used to align the gate pulses and the optical pulses. Tunable electronic delays after detection were used to shift the coincidence peak in the histogram away from zero delay to avoid any loss of counts.

To show the enhancement of our scheme, we measured the CAR and coincidence rate at different input power levels. As a reference, we performed measurements with only P1 or P2 turned on, each operating at 50 MHz. We then took TWDM measurements at the same conditions. The results are plotted in Fig. 4, which shows a coincidence rate (i.e., heralded single photon rate) improvement of $90 \pm 5\%$, with a decrease of $14 \pm 2\%$ in CAR. In the single-pump measurements (blue squares and purple circles), increasing the coincidence rate by the same amount would typically reduce the CAR by 40%, as the result of multi-pair generation with increased pump power.

To compare the performance of this TWDM scheme with that of simply doubling the repetition rate of a single pump through TDM, we performed a single-pump experiment operating at 100 MHz. The results are plotted in Fig. 4. The two sets of experimental results almost overlap at high power, showing that the TWDM source offers a similar performance in this power range. However, the CAR in the TWDM experiment is lower than that in the single-pump experiment at low power. We attribute this to the cross talk between the photons generated from two pumps and different dark count rates for the two schemes due to the inherent differences in triggering the ID210 detectors.

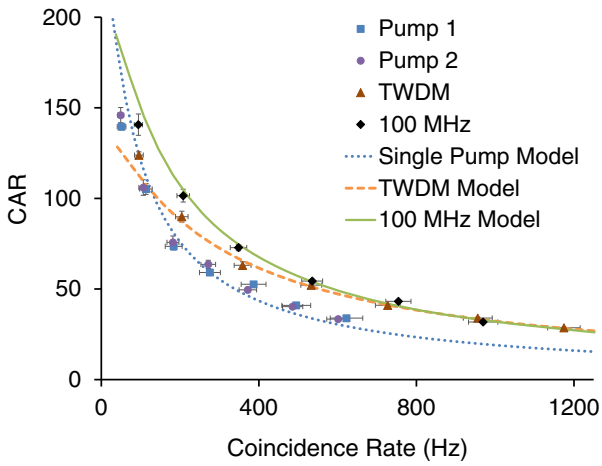

Fig. 4. Measured CAR as a function of true coincidence rate. Blue squares and purple circles represent the results with only P1 or P2 turned on, respectively; brown traingles represent the TWDM results. Measurements with only one pump at 100 MHz are shown for comparison (black diamonds). The measurement beyond 950-Hz coincidence rate for the 100-MHz pump could not be done because of the detector saturation. The dotted blue, dashed orange, and solid green lines represent analytical models [15] based on experimental parameters for a single pump, TWDM, and 100-MHz pump, respectively. Poissonian error bars are included.

Ideally, this TWDM source should offer 100% enhancement to the heralded single-photon rate without reducing the CAR, because the two pumps were not temporally overlapped and should behave like pumping the nanowire independently. In reality, however, the ID210 detectors used to detect signal photons were gated by their pumps, and the effective gate pulse width had to be no less than 1 ns to get reasonable counts. Even though the 1 ns gate width is much less than the 10 ns separation between the multiplexed pulses, we found that the detector synchronized to one pump could capture signal photons generated from the other pump. For example, when we only switched ECDL1 on, the detector ID210-2 wasn't meant to have any counts beyond dark count. However, because P1 could also generate photons at the S2 wavelength and the gate pulses for ID210-2 were measured to have a small hump that was temporally overlapped with P1, we observed some photon counts beyond dark counts. These counts got into the TIA through the OR gate and contributed to accidentals, because the S2 photons generated by P1 would not be correlated with the idler photons generated by P1. We found similar noise increase when we only switched ECDL2 on. Therefore, when we switched both lasers on for the TWDM source, the two pump channels were not completely independent, but had cross talk through the detectors because of a charge persistence effect introduced through imperfect gating [20]. When a large amount of photons are illuminated on an APD while the gate is OFF, there is still a probability to generate electrons in the active area of the APD because the gate pulse voltage is not actually zero. Once the gate is switched ON in a few ns, these electrons will generate electrical pulses and give some counts. In the low-power regime, because the true photon rate is low and therefore is very sensitive to noise, the cross talk

noise affects the CAR more significantly than in the high-power regime. This explains why the two plots overlap at high power, but diverge at low power.

The benefit of this TWDM scheme is to avoid the avalanche detector saturation introduced by the detector deadtime. As the deadtime of the detectors in our experiment was set to 20 μs to reduce the afterpulsing noise, the maximum count rate allowed by this deadtime was 50 kHz. This limited the maximum measurable coincidence rate to 950 Hz when using a single pump with 100-MHz repetition rate (Fig. 4). The ratio of 950/50000 corresponded to the 17 dB loss in the heralded (idler) channel. In contrast, the coincidence rate in the new scheme is nearly 1200 Hz (Fig. 4), breaking the limit by distributing the heralding photons to multiple wavelength channels. The detector for the idler channel in our experiment was a SSPD with a deadtime of only tens of nanoseconds and thus did not have a saturation problem. We point out that the reason of using the SSPD here for the idler channel was because we did not have a third APD. In the case that an APD is used for the idler channel, one can use the output of the OR gate from the heralding channels to trigger the APD and avoid saturation, as shown in Fig. 1(b).

We point out that this TWDM scheme for silicon nanowire-based heralded photon sources can be scaled up once the imperfect gating issue is solved. One solution is to make the gate pulse voltage as close to zero as possible when the gate is OFF. To make full use of the SFWM bandwidth, AWGs with 0.05-THz channel spacing and 0.025-THz channel bandwidth will be required to multiplex more wavelength channels. Such AWGs are commercially available, and for telecom C-band wavelengths, there are 80 channels. This allows for scaling the TWDM scheme up to 14 pumps before the pumps are too close to the photon channels and will cause contamination. The SFWM bandwidth required for multiplexing 14 pumps is only 2 THz, well within the SFWM bandwidth provided by the silicon nanowire. Because the active temporal-multiplexing scheme that was proposed to increase μ is based on time-division multiplexing [13], our TWDM scheme will form the foundation of active temporal multiplexing at high photon rates.

In conclusion, we have proposed and demonstrated a TWDM scheme to enhance the heralded single-photon rate from a silicon nanowire. We have shown that a $90 \pm 5\%$ enhancement on the heralded photon rate can be achieved at the cost of only $14 \pm 2\%$ reduction to CAR. The drop in CAR at low power is due to the cross talk between the two pumps when using them to trigger the APDs. This cross talk was caused by imperfect detector gating, which is not an intrinsic problem to this TWDM scheme. Most importantly, as heralding photons generated by different pumps are detected with separate APDs, the performance of this scheme is not limited by detector saturation because the repetition rate of each pump is fixed.

We would like to thank Matthew Collins for discussion and providing support in using the TIA. We acknowledge funding support from the Centre of Excellence (CUDOS, CE110001018), Laureate Fellowship (FL120100029), Future Fellowship (FT110100853), Discovery Project (DP130100086) and Discovery Early Career Researcher Award (DE130101148 and DE120100226) programs of the Australian Research Council (ARC).

References

1. E. Knill, R. Laflamme, and G. L. Milburm, Nature **409**, 46 (2006).
2. H. J. Kimble, Nature **453**, 1023 (2008).
3. O. Alibart, D. B. Ostrowsky, P. Baldi, and S. Tanzilli, Opt. Lett. **30**, 1539 (2005).
4. M. Lobino, G. D. Marshall, C. Xiong, A. S. Clark, D. Bonneau, C. M. Natarajan, M. G. Tanner, R. H. Hadfield, S. N. Dorenbos, T. Zijlstra, V. Zwiller, M. Marangoni, R. Ramponi, M. G. Thompson, B. J. Eggleton, and J. L. O'Brien, Appl. Phys. Lett. **99**, 081110 (2011).
5. J. E. Sharping, K. F. Lee, M. A. Foster, A. C. Turner, B. S. Schmidt, M. Lipson, A. L. Gaeta, and P. Kumar, Opt. Express **14**, 12388 (2006).
6. K. Harada, H. Takesue, H. Fukuda, T. Tsuchizawa, T. Watanabe, K. Yamada, Y. Tokura, and S. Itabashi, IEEE J. Sel. Top. Quantum Electron. **16**, 325 (2010).
7. M. J. Collins, A. S. Clark, J. He, D.-Y. Choi, R. J. Williams, A. C. Judge, S. J. Madden, M. J. Withford, M. J. Steel, B. Luther-Davies, C. Xiong, and B. J. Eggleton, Opt. Lett. **37**, 3393 (2012).
8. C. Xiong, C. Monat, M. J. Collins, L. Tranchant, D. Petiteau, A. S. Clark, C. Grillet, G. D. Marshall, M. J. Steel, J. Li, L. O'Faolain, T. F. Krauss, and B. J. Eggleton, IEEE J. Sel. Top. Quantum Electron. **18**, 1676 (2012).
9. M. Davanço, J. R. Ong, A. B. Shehata, A. Tosi, I. Agha, S. Assefa, F. Xia, W. M. J. Green, S. Mookherjea, and K. Srinivasan, Appl. Phys. Lett. **100**, 261104 (2012).
10. N. Matsuda, H. Takesue, K. Shimizu, Y. Tokura, E. Kuramochi, and M. Notomi, Opt. Express **21**, 8596 (2013).
11. A. S. Clark, C. Husko, M. J. Collins, G. Lehoucq, S. Xavier, A. De Rossi, S. Combrié, C. Xiong, and B. J. Eggleton, Opt. Lett. **38**, 649 (2013).
12. A. L. Migdall, D. Branning, and S. Castelletto, Phys. Rev. A **66**, 053805 (2002).
13. J. Mower and D. Englund, Phys. Rev. A **84**, 052326 (2011).
14. X.-S. Ma, S. Zotter, J. Kofler, T. Jennewein, and A. Zeilinger, Phys. Rev. A **83**, 043814 (2011).
15. M. J. Collins, C. Xiong, I. H. Rey, T. D. Vo, J. He, S. Shahnia, C. Reardon, M. J. Steel, T. F. Krauss, A. S. Clark, and B. J. Eggleton, Nat. Commun. **4**, 2582 (2013).
16. D. Bonneau, G. J. Mendoza, J. L. O'Brien, and M. G. Thompson, arXiv: 1409.5341, (2014).
17. M. A. Broome, M. P. Almeida, A. Fedrizzi, and A. G. White, Opt. Express **19**, 22698 (2011).
18. K. Harada, H. Takesue, H. Fukuda, T. Tsuchizawa, T. Watanabe, K. Yamada, Y. Tokura, and S. Itabashi, New J. Phys. **13**, 065005 (2011).
19. Q. Lin and G. P. Agrawal, Opt. Lett. **31**, 3140 (2006).
20. J. Zhang, R. Thew, J.-D. Gautier, N. Gisin, and H. Zbinden, IEEE J. Quantum Electron. **45**, 792 (2009).